WATER RESOURCES RESEARCH, VOL. 28, NO. 3, PAGES 925–938, MARCH 1992

Gravity-Driven Groundwater Flow and Slope Failure Potential 1. Elastic Effective-Stress Model

RICHARD M. IVERSON AND MARK E. REID[1]

U.S. Geological Survey, Cascades Volcano Observatory, Vancouver, Washington

Hilly or mountainous topography influences gravity-driven groundwater flow and the consequent distribution of effective stress in shallow subsurface environments. Effective stress, in turn, influences the potential for slope failure. To evaluate these influences, we formulate a two-dimensional, steady state, poroelastic model. The governing equations incorporate groundwater effects as body forces, and they demonstrate that spatially uniform pore pressure changes do not influence effective stresses. We implement the model using two finite element codes. As an illustrative case, we calculate the groundwater flow field, total body force field, and effective stress field in a straight, homogeneous hillslope. The total body force and effective stress fields show that groundwater flow can influence shear stresses as well as effective normal stresses. In most parts of the hillslope, groundwater flow significantly increases the Coulomb failure potential Φ, which we define as the ratio of maximum shear stress to mean effective normal stress. Groundwater flow also shifts the locus of greatest failure potential toward the slope toe. However, the effects of groundwater flow on failure potential are less pronounced than might be anticipated on the basis of a simpler, one-dimensional, limit equilibrium analysis. This is a consequence of continuity, compatibility, and boundary constraints on the two-dimensional flow and stress fields, and it points to important differences between our elastic continuum model and limit equilibrium models commonly used to assess slope stability.

INTRODUCTION

The gravitational attraction of the Earth drives both groundwater movement and deformation in many rocks and soils. A direct consequence of this gravitational attraction is topographic control of groundwater flow systems and rock or soil stresses that can lead to slope failures and some types of crustal faulting. Although the influences of topography on groundwater flow and subsurface stresses have been analyzed separately [e.g., *Toth*, 1963; *Freeze and Witherspoon*, 1966, 1967; *Savage et al.*, 1985], there has been a lack of results that show how topography simultaneously influences groundwater flow and effective stress fields that, in turn, influence failure potential. This lack is surprising in light of the almost universal acceptance of *Terzaghi*'s [1923, 1936] effective stress principle. Moreover, the lack has represented a missing link in the chain of principles that unite hydrology and geomorphology.

This paper and its companion [*Reid and Iverson*, this issue] provide quantitative results that show how topographically controlled groundwater flow influences the Coulomb failure potential in hillslopes and mountain massifs. In both papers we restrict our attention to two-dimensional, periodic topography, which forms repetitious landscapes composed of identical, symmetrical ridges and valleys of infinite length (Figure 1). The landscapes are saturated with groundwater that undergoes steady Darcian flow. Groundwater flow and slope failure potential in such simple landscapes are scale independent, a characteristic that is lacking if partially saturated conditions are considered. Even for these simple landscapes, however, the two-dimensional topography renders the effective stress field statically indeterminate. That is, there are more stress components than can be determined from the equations of equilibrium alone. Consequently, more assumptions are needed to calculate the effective stress field and slope failure potential than in analogous one-dimensional problems [e.g., *Iverson and Major*, 1986].

To overcome the problem of static indeterminacy, we assume that rock or soil deformation prior to failure is infinitesimal and linearly elastic. This approach differs markedly from that used in conventional, limit equilibrium analyses of slope stability. Such analyses do not employ a constitutive model (such as linear elasticity) and do not determine effective stress and deformation fields. Instead, they determine the net forces and factor of safety along assumed failure surfaces by making assumptions about the forces or moments acting between vertical slices of rock or soil [e.g., *Wright et al.*, 1973; *Nash*, 1987]. Here, in contrast, we use a comprehensive mathematical model to quantify how groundwater flow influences effective stresses and slope failure potential; we do not assess failure surface locations or factors of safety.

This paper begins with a brief review of the methods and results of pertinent previous work. Then in presenting the necessary mathematical formulation it focuses on the physical principles and assumptions embodied in our model. Our formulation particularly emphasizes the definition of effective stress, which has been a source of some controversy [e.g., *Passman and McTigue*, 1986]. We show that standard, elastic effective stress calculations can be interpreted in the context of a standard, Coulomb failure rule only if specific assumptions are made. Next, we present numerical results for an elementary two-dimensional problem, which illustrates how groundwater flow influences the effective stress field and Coulomb failure potential in slopes. We contrast these results with those from a statically determinate, one-dimensional limit equilibrium calculation for a similar slope, and we discuss the implications and limitations of our findings. In the companion paper [*Reid and Iverson*, this issue] we consider more complicated problems and their

[1]Now at U.S. Geological Survey, Honolulu, Hawaii.

Paper number 91WR02694.

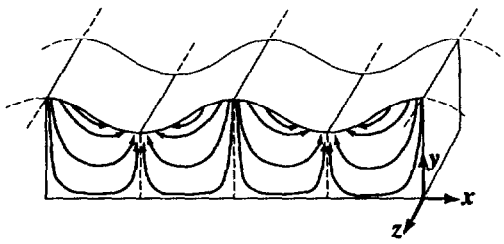

Fig. 1. Schematic block diagram of an infinitely extensive landscape with periodic topography. Streamlines show paths of gravity-driven groundwater flow.

geomorphological implications; we present numerical results for hillslopes with diverse shapes, material properties, and hydraulic heterogeneities.

Related Work

Many investigators have examined the influence of topography on steady, gravity-driven groundwater flow fields. One modeling approach assumes that the water table mimics topography. Two-dimensional analytical and numerical solutions using this approach show that recharge areas with hydraulic gradients directed downward occur in topographically higher regions, whereas discharge areas occur in lower regions [*Toth*, 1963; *Freeze and Witherspoon*, 1966, 1967]. A more sophisticated approach treats the water table as a free surface that can vary with changes in flow system characteristics, such as hydraulic conductivity or infiltration rate. *Forster and Smith* [1988*a*, *b*] used this approach to simulate steady groundwater flow in mountainous terrain, where the water table might not correspond with the ground surface. However, their numerical solutions indicate that in humid climates the water table is at or near the ground surface.

Other workers have noted that realistic groundwater flow fields can strongly influence the potential for slope instability determined by conventional limit equilibrium methods [e.g., *Hodge and Freeze*, 1977; *Rulon and Freeze*, 1985] as well as instability observed in the field [e.g., *Patton and Hendron*, 1974; *Iverson and Major*, 1987; *Reid et al.*, 1988]. The statically determinate infinite slope analysis of *Iverson and Major* [1986] showed how both the direction and magnitude of groundwater hydraulic gradients influence the potential for instability.

The gravitational state of stress induced by topography has also attracted the interest of numerous investigators. Many have used a linearly elastic constitutive assumption to model the stress state in dry earth materials that experience a uniform gravitational body force. A variety of two-dimensional analytical solutions [e.g., *Perloff et al.*, 1967; *McTigue and Mei*, 1981; *Silvestri and Tabib*, 1983*a*, *b*; *Savage et al.*, 1985] and numerical solutions [e.g., *Duncan and Dunlop*, 1969; *Phukan et al.*, 1970; *Hoyaux and Landanyi*, 1972; *Sturgul et al.*, 1976] to static boundary value problems have been presented. These solutions clearly show that both the magnitude and orientation of stresses in hillslopes are affected by topography.

Other workers have used the assumption of linear elasticity to examine two-dimensional effective stress fields in saturated materials in which both solids and fluids experience gravitational body forces. In time-dependent problems, fluid flow is fully coupled with deformation [*Sandhu and Wilson*, 1969; *Zienkiewicz et al.*, 1977]. With steady state groundwater flow and static stresses the flow field is decoupled from deformation (Appendix A), and the effective stress distribution can be calculated by using either a pore pressure or seepage force distribution [*Ter-Martirosyan and Akhpatelov*, 1971; *Zienkiewicz*, 1977; *Zienkiewicz et al.*, 1977; *Louis et al.*, 1977]. Results from both transient and steady flow problems clearly demonstrate that hydraulic gradients influence the effective stress distribution. However, no previous studies have systematically examined the effects we consider here, those of gravity-driven groundwater flow controlled by topography.

Mathematical Formulation

Beginning with *Biot* [1941], many authors have presented formulations of the basic equations governing pore pressures, elastic stresses, and infinitesimal strains in quasi-static porous media with Darcian fluid flow [e.g., *Serafim*, 1968; *Cooley*, 1975; *Rice and Cleary*, 1976]. Here we develop a simple, steady flow formulation that employs hydraulic head rather than pore pressure as the basic fluid variable. This helps distinguish groundwater effects from elastic deformation effects and reveals the importance of spatial patterns of groundwater flow. Our governing equations also highlight the role of gravitational potential and body forces, whereas many works on poroelasticity ignore the gravitational potential of pore fluid, and some well-known works, such as those of *Biot* [1941] and *Rice and Cleary* [1976], also omit body forces due to the weight of the solid constituents. Although this omission may be useful in addressing some problems, it is clearly inappropriate for hillslopes. In our formulation we assume that the pore water is isothermal and has a uniform density and viscosity and that the solid porous medium is isothermal and isotropic, both elastically and hydraulically; and we restrict our attention to plane strain and two-dimensional groundwater flow. Extension of our formulation to three dimensions is simple, however, and is parallel to classical, three-dimensional, elastic equilibrium formulations [e.g., *Timoshenko and Goodier*, 1970].

Displacement, Strain, and Compatibility

The most fundamental equations we use are those that define infinitesimal strains in the solid porous medium in terms of displacement gradients [e.g., *Fung*, 1965; *Malvern*, 1969]:

$$\varepsilon_{xx} = \frac{\partial u_x}{\partial x} \tag{1a}$$

$$\varepsilon_{yy} = \frac{\partial u_y}{\partial y} \tag{1b}$$

$$\varepsilon_{yx} = \frac{1}{2}\left(\frac{\partial u_x}{\partial y} + \frac{\partial u_y}{\partial x}\right) \tag{1c}$$

Here x and y are rectangular Cartesian coordinates, u_x and u_y are the components of the solid displacement in the x and y directions, ε_{xx} and ε_{yy} define normal strains in these directions, and ε_{yx} is the shear strain in the x direction on planes normal to y. Owing to symmetry of the strain tensor, shear strains on orthogonal planes are equal: $\varepsilon_{yx} = \varepsilon_{xy}$.

Equations (1*a*)–(1*c*) are valid regardless of stress definitions or material behavior. They play an important role in the problems we consider, because boundary conditions and governing equations are specified in terms of the solid displacements.

Differentiating and combining (1*a*)–(1*c*) lead directly to a single equation of strain compatibility, which expresses a kinematic continuity constraint on the displacement and strain fields [*Timoshenko and Goodier*, 1970, p. 29]:

$$\frac{\partial^2 \varepsilon_{xx}}{\partial y^2} + \frac{\partial^2 \varepsilon_{yy}}{\partial x^2} = 2\,\frac{\partial^2 \varepsilon_{yx}}{\partial x \partial y} \tag{2}$$

Stress Equilibrium

The equations of static, total stress equilibrium for the solid-fluid mixture also are valid regardless of the solid or fluid rheology. In a porous medium with steady fluid flow, stresses are independent of time and the equations have the form of the traditional Cauchy equations for a static continuum [e.g., *Fung*, 1965; *Malvern*, 1969]:

$$\frac{\partial \sigma_{xx}}{\partial x} + \frac{\partial \sigma_{yx}}{\partial y} = -\rho_t g_x \tag{3a}$$

$$\frac{\partial \sigma_{yy}}{\partial y} + \frac{\partial \sigma_{yx}}{\partial x} = -\rho_t g_y \tag{3b}$$

Here σ_{xx} and σ_{yy} are the total normal stresses acting on planes normal to the x and y axes, respectively, and σ_{yx} is the shear stress acting on each of these planes. The stress tensor, like the strain tensor, is symmetric. Normal stresses are defined as positive in tension. The components of gravitational acceleration in the x and y directions are g_x and g_y, respectively, and ρ_t is the bulk density of the solid-fluid mixture.

Effective Stress

We adopt a general definition of effective stress σ'_{ij}:

$$\sigma'_{ij} = \sigma_{ij} + \alpha p \delta_{ij} \tag{4}$$

Here p is the pore water pressure, δ_{ij} is the Kronecker delta, and i and j are indices that represent x or y. The value of the coefficient α has been the subject of longstanding controversy, dating to *Terzaghi*'s [1923] development of the effective stress concept. Some authors, such as *Hubbert and Rubey* [1959], have attempted to prove theoretically that $\alpha = 1$. Other authors have maintained that, if all strains are elastic, it is necessary that $\alpha = 1 - K_b/K_s$, where K_s and K_b are the elastic bulk moduli of the individual solid grains and the solid porous medium, respectively [*Nur and Byerlee*, 1971]. Still others, including Terzaghi, have argued on theoretical grounds that α should depend on the porosity or porous structure of the solid matrix [*Serafim*, 1968]. *Passman and McTigue* [1986] have developed a more comprehensive definition of effective stress that is consistent with the continuum theory of mixtures. However, their definition reduces to (4) with $\alpha = 1$ if fluid flow is steady, and all viscous energy dissipation is Darcian. For the present, we simply adopt the effective stress definition of (4), in which the value of α is unspecified. We later show that the values $\alpha = 1$ and $\alpha = 1 - K_b/K_s$ must be reconciled for elastic stresses to be interpreted in the context of a Coulomb failure rule.

Effective Stress Equilibrium

Substituting (4) into (3) yields effective stress equilibrium equations with pore pressure gradient terms that play the role of body forces:

$$\frac{\partial \sigma'_{xx}}{\partial x} + \frac{\partial \sigma'_{yx}}{\partial y} = -\rho_t g_x + \alpha\,\frac{\partial p}{\partial x} \tag{5a}$$

$$\frac{\partial \sigma'_{yy}}{\partial y} + \frac{\partial \sigma'_{yx}}{\partial x} = -\rho_t g_y + \alpha\,\frac{\partial p}{\partial y} \tag{5b}$$

We choose the y coordinate to be directed vertically upward, with an origin at an arbitrary horizontal datum (Figure 1). Thus gravity acts exclusively in the negative y direction, and we define the hydraulic head h as

$$h = \frac{p}{\rho_w g} + y \tag{6}$$

in which ρ_w is the pore water density and g is the magnitude of gravitational acceleration. Solving (6) for p and substituting into (5*a*) and (5*b*) yields effective stress equilibrium equations that contain head gradient terms and a submerged-unit-weight term as body forces:

$$\frac{\partial \sigma'_{xx}}{\partial x} + \frac{\partial \sigma'_{yx}}{\partial y} = \alpha \rho_w g\,\frac{\partial h}{\partial x} \tag{7a}$$

$$\frac{\partial \sigma'_{yy}}{\partial y} + \frac{\partial \sigma'_{yx}}{\partial x} = (\rho_t - \alpha \rho_w) g + \alpha \rho_w g\,\frac{\partial h}{\partial y} \tag{7b}$$

The submerged-unit-weight term $(\rho_t - \alpha\rho_w)g$ represents the hydrostatic buoyancy effects of the pore fluid, whereas the head gradient terms represent the seepage force associated with pore fluid flow.

Effective Stress and Elastic Strain

To determine the three unknown stress components in the two equilibrium equations (7*a*) and (7*b*), it is necessary to employ constitutive equations that relate stresses to strains in the solid porous medium. We adopt the widely accepted constitutive equations for porous elastic media that were developed by *Biot* [1941]. Biot used arguments about the strain energy in an infinitesimally deformed poroelastic body to derive general, linear, isotropic constitutive equations in terms of total stresses and pore pressure. *Rice and Cleary* [1976] subsequently recast his equations in a form that accounts for the compressibility of both solid and fluid constituents in terms of conventional elastic moduli. In turn, we have recast these equations in a form that facilitates their comparison with a standard form of Hooke's law for linearly elastic behavior (Appendix B).

The Biot-type constitutive equations for total stress (B7*a*)–(B7*c*) reduce to standard Hooke's-law-type equations for effective stress only if the definition $\alpha = 1 - K_b/K_s$ advocated by *Nur and Byerlee* [1971] is adopted. In this event, (4) becomes

$$\sigma'_{ij} = \sigma_{ij} + \left(1 - \frac{K_b}{K_s}\right) p\delta_{ij} \tag{8}$$

and standard Hooke's law constitutive equations then result from substitution of (8) into (B7a)–(B7c):

$$\varepsilon_{xx} = \frac{1}{E}[(1 - \nu^2)\sigma'_{xx} - \nu(1 + \nu)\sigma'_{yy}] \tag{9a}$$

$$\varepsilon_{yy} = \frac{1}{E}[(1 - \nu^2)\sigma'_{yy} - \nu(1 + \nu)\sigma'_{xx}] \tag{9b}$$

$$\varepsilon_{yx} = \frac{1 + \nu}{E}\sigma'_{yx} \tag{9c}$$

Here E is the Young's modulus and ν is the drained Poisson's ratio of the solid porous medium. Note that, as a consequence of (8), $\sigma'_{ij} = \sigma_{ij}$ when $i \neq j$, and shear stresses can be regarded as either total or effective stresses. The plane strain constraint,

$$\sigma'_{zz} = \nu(\sigma'_{xx} + \sigma'_{yy}) \tag{10}$$

is implicit in (9a)–(9c). Equations (9) and (10) are identical to standard elasticity equations [*Timoshenko and Goodier*, 1970, pp. 17 and 30], except that the relevant stresses here are effective stresses. This implies that effective stress alone drives elastic deformation of the solid porous medium, consistent with the ideas of *Terzaghi* [1936].

Equation (8) consequently represents the definition of effective stress that is most convenient for problems involving elastic deformation of porous media. It gives effective stress equilibrium problems the form of conventional linear-elasticity problems, and it allows groundwater effects to enter the formulation only through the body force terms in the equilibrium equations [cf. *Rice and Cleary*, 1976]. There is nothing exclusive or fundamentally superior, however, about the effective stress definition given by (8). This has been pointed out by others [*Stagg and Zienkiewicz*, 1968; *Cooley*, 1975], with the caveat that any value of α can be used in effective stress equilibrium calculations, as long as total stress equilibrium is satisfied. Nevertheless, any definition of effective stress other than that of (8) produces elastic constitutive equations that have an unconventional form, which mixes the effects of porous medium elasticity with those of groundwater flow.

Coulomb Failure and Effective Stress

Because we wish to assess the potential for Coulomb failure that results from stress field modification by groundwater flow, we must question whether the effective stress definition of (8) is appropriate in the context of the Coulomb failure rule. This rule is founded purely on observations, which indicate that the effective stress definition most useful for describing Coulomb failure of earth materials is simply [*Jaeger and Cook*, 1979, p. 223]:

$$\sigma'_{ij} = \sigma_{ij} + p\delta_{ij} \tag{11}$$

The discrepancy between this effective stress definition (11) and that used in our poroelastic stress calculations (8) can be eliminated if we assume that the constituent particles composing the solid porous medium are much less compressible than is the porous medium as a whole (i.e., $K_b \ll K_s$). Then $\alpha \approx 1$, and (8) is made to approximate (11). In this case, (9a)–(9c) remain valid and reconcilable with the Biot-type equations (Appendix B), but the effective stresses that are calculated using (9a)–(9c) can be interpreted in the context of Coulomb failure potential. Because we adopt the assumption $K_b \ll K_s$, we restrict the generality of our formulation somewhat, but we remove any ambiguity from our methodology and results.

Effective Stress Compatibility

The equation of effective stress compatibility completes the set of equations governing the effective stress field. To obtain this equation, we assume that the elastic moduli are constant but that the total bulk density (which depends on both the density of the solids and the porosity) and the hydraulic conductivity may vary spatially. Substituting the effective stress constitutive equations (9a)–(9c) into the strain compatibility equation (2) yields, after some algebraic manipulation,

$$\frac{\partial^2}{\partial y^2}[(1 - \nu)\sigma'_{xx} - \nu\sigma'_{yy}] + \frac{\partial^2}{\partial x^2}[(1 - \nu)\sigma'_{yy} - \nu\sigma'_{xx}] = 2\frac{\partial^2 \sigma'_{yx}}{\partial x \partial y} \tag{12}$$

Adopting the definition $\alpha = 1$ (i.e., $K_b \ll K_s$), differentiating (7a) with respect to x, differentiating (7b) with respect to y, and combining the resulting equations yields

$$\frac{\partial^2 \sigma'_{xx}}{\partial x^2} + \frac{\partial^2 \sigma'_{yy}}{\partial y^2} + 2\frac{\partial^2 \sigma'_{yx}}{\partial x \partial y} - \rho_w g\left(\frac{\partial^2 h}{\partial x^2} + \frac{\partial^2 h}{\partial y^2}\right) - g\frac{\partial \rho_t}{\partial y} = 0 \tag{13}$$

Adding (12) and (13) then yields the compatibility equation in terms of effective stresses and hydraulic head gradients:

$$\left(\frac{\partial^2}{\partial x^2} + \frac{\partial^2}{\partial y^2}\right)(\sigma'_{xx} + \sigma'_{yy}) = \frac{1}{1 - \nu} \cdot \left[\rho_w g\left(\frac{\partial^2 h}{\partial x^2} + \frac{\partial^2 h}{\partial y^2}\right) + g\frac{\partial \rho_t}{\partial y}\right] \tag{14}$$

If the bulk density and hydraulic conductivity of the porous medium are uniform, the right-hand side of (14) equals zero ($\nabla^2 h = 0$ for steady groundwater flow in a homogenous, isotropic medium). Equation 14 then has the same form as the conventional compatibility equation used in plane strain elasticity [*Timoshenko and Goodier*, 1970, p. 31]. If the hydraulic conductivity is nonuniform, however, (14) shows that the groundwater flow field will influence the effective stress field in a manner that has no direct analog in standard elasticity problems. This leads to particularly interesting effective stress distributions in the vicinity of hydraulic heterogeneities [*Reid and Iverson*, this issue].

Groundwater Flow

The equation for steady, two-dimensional groundwater flow is independent of the equations describing static effective stresses and infinitesimal elastic strains (Appendix A). Consequently, we assume that there is an arbitrary hydraulic

conductivity distribution, but we do not specify an explicit relation between strains and conductivities. Thus we use the conventional equation for steady, two-dimensional groundwater flow in a porous medium that is hydraulically isotropic but not necessarily homogeneous:

$$\frac{\partial}{\partial x}\left(K\frac{\partial h}{\partial x}\right)+\frac{\partial}{\partial y}\left(K\frac{\partial h}{\partial y}\right)=0 \tag{15}$$

in which K is the scalar-valued hydraulic conductivity [cf. *Freeze and Cherry*, 1979, p. 64]. We use the solution of this equation to determine the hydraulic head gradients in (7*a*), (7*b*), and (14).

Displacement Formulation

Combined with appropriate boundary conditions, the effective stress problem posed by (7*a*), (7*b*), (14), and (15) is mathematically complete, but a difficulty exists because the periodic topography dictates that boundary conditions for the solid phase must be expressed in terms of displacements rather than stresses. Thus we recast the governing equations in terms of displacements. First, we express the constitutive equations in terms of displacements by substituting (1*a*)–(1*c*) into (9*a*)–(9*c*) and manipulating the result to obtain

$$\sigma'_{xx}=\frac{E}{1+\nu}\left(\frac{\partial u_x}{\partial x}\right)+\frac{\nu E}{(1-2\nu)(1+\nu)}\left(\frac{\partial u_x}{\partial x}+\frac{\partial u_y}{\partial y}\right) \tag{16a}$$

$$\sigma'_{yy}=\frac{E}{1+\nu}\left(\frac{\partial u_y}{\partial y}\right)+\frac{\nu E}{(1-2\nu)(1+\nu)}\left(\frac{\partial u_y}{\partial y}+\frac{\partial u_x}{\partial x}\right) \tag{16b}$$

$$\sigma'_{yx}=\frac{E}{2(1+\nu)}\left(\frac{\partial u_x}{\partial y}+\frac{\partial u_y}{\partial x}\right) \tag{16c}$$

Substitution of (16*a*)–(16*c*) into the effective stress equilibrium equations (7*a*) and (7*b*) with $\alpha = 1$, followed by further algebraic manipulation, results in two equations for the two components of displacement, u_x and u_y:

$$\frac{E}{2(1+\nu)}\nabla^2 u_x+\left[\frac{\nu E}{(1-2\nu)(1+\nu)}+\frac{E}{2(1+\nu)}\right]\cdot\left(\frac{\partial^2 u_x}{\partial x^2}+\frac{\partial^2 u_y}{\partial y\partial x}\right)=\rho_w g\frac{\partial h}{\partial x} \tag{17a}$$

$$\frac{E}{2(1+\nu)}\nabla^2 u_y+\left[\frac{\nu E}{(1-2\nu)(1+\nu)}+\frac{E}{2(1+\nu)}\right]\cdot\left(\frac{\partial^2 u_y}{\partial y^2}+\frac{\partial^2 u_x}{\partial x\partial y}\right)=(\rho_t-\rho_w)g+\rho_w g\frac{\partial h}{\partial y} \tag{17b}$$

The coefficient groups, $\nu E/[(1-2\nu)(1+\nu)]$ and $E/2(1+\nu)$, which appear in (17*a*) and (17*b*), can be identified as the Lamé parameters of the conventional theory of linear elasticity [*Fung*, 1965].

Note that in (17*a*) and (17*b*), as well as in the equations governing the groundwater flow and effective stress fields, the consequence of a uniform pore pressure change is zero, because such a change leaves $\partial h/\partial x$ and $\partial h/\partial y$ unchanged. This shows that (17*a*) and (17*b*) can be applied, without modification, to materials with no groundwater flow, or, if ρ_w is set equal to 0, to materials with no pore water. It also demonstrates that spatially uniform pore pressure increases do not make rocks and soils more prone to failure. We consider this inference further when we discuss the solutions of boundary value problems.

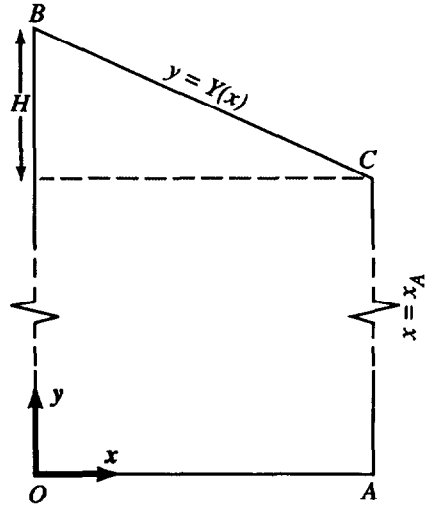

Fig. 2. Geometry of the solution domain for the example problem. Right and left boundaries are symmetry boundaries dictated by periodic topography. The height of the solution domain is $10H$ and is shown in compressed form.

Boundary Conditions

Each of the boundary conditions necessary to solve (15), (17*a*), and (17*b*) reflects one of three basic premises: (1) that the surface topography is periodic; (2) that there are no forces acting on the topographic surface; (3) that the influence of the bottom boundary on displacements, stresses and groundwater flow near the topographic surface is inconsequential if the bottom boundary is at a large but finite depth.

We specify the boundary conditions for solid displacements with reference to Figure 2. The periodic topography premise requires that there is no horizontal displacement of the lateral margins of the domain, O-B and A-C. Stated mathematically, these conditions are

$$u_x(0,\ y)=0 \tag{18a}$$

$$u_x(x_A,\ y)=0 \tag{18b}$$

We quantify the premise of a finite bottom boundary depth by specifying zero vertical displacement along O-A (Figure 2):

$$u_y(x,\ 0)=0 \tag{18c}$$

The final boundary condition for displacements arises from the requirement that there is no force acting on the topographic surface. The surface is consequently a traction-free boundary [*Malvern*, 1969, p. 499], and for plane strain this requires that

$$\sigma'_{xx}(x,\ Y)n_x+\sigma'_{yx}(x,\ Y)n_y=0 \tag{18d}$$

$$\sigma'_{yy}(x,\ Y)n_y+\sigma'_{yx}(x,\ Y)n_x=0 \tag{18e}$$

in which n_x and n_y are the x and y components of the unit normal vector directed outward from the topographic sur-

face and Y is the value of y on the surface. Substitution of (16a)–(16c) into (18d) and (18e) results in the traction-free boundary equations expressed in terms of displacements. These equations are easy to obtain but are very lengthy, so we omit them here.

For groundwater flow the periodic topography premise leads to no-flow boundaries on the lateral margins O-B and A-C of Figure 2:

$$\frac{\partial h}{\partial x}(0, y) = 0 \tag{19a}$$

$$\frac{\partial h}{\partial x}(x_A, y) = 0 \tag{19b}$$

A no-flow boundary condition is also appropriate for the deep bottom boundary along O-A of Figure 2:

$$\frac{\partial h}{\partial y}(x, 0) = 0 \tag{19c}$$

Finally, the boundary condition along the topographic surface specifies that the head at any point on the surface is equal to the elevation of that point:

$$h(x, Y) = Y \tag{19d}$$

Numerical Solution

Our method of solving the problem posed by (15), (17a), (17b), (18a)–(18e), and (19a)–(19d) employs two Galerkin finite element models, one for groundwater flow and another for elastic displacements. For dry hillslopes the body force field is uniform, and the displacement equations (17a) and (17b) have hydraulic gradients, $\partial h/\partial x$ and $\partial h/\partial y$, and pore water density ρ_w equal to zero. In this case we use the elastic stress-strain code DLEARN [*Hughes*, 1987] to obtain approximate displacement solutions. This code incorporates bilinear, four-node, quadrilateral, isotropic, elastic continuum elements. Once displacements at each node are obtained, we calculate average strains for each element using (1a)–(1c). We then find effective stresses by applying the appropriate form of Hooke's law (16a)–(16c).

For saturated hillslopes our first step in computing effective stresses is to find the steady state hydraulic head distribution described by (15). We use the groundwater flow code MODFE [*Torak*, 1992] to approximate this distribution. This code employs linear, three-node, triangular elements. On the basis of the simulated head distribution we then compute hydraulic gradients for each element using the methods described by *Pinder et al.* [1981]. We determine the body forces (due to both gravity and seepage) acting on each stress quadrilateral using weighted averages of the triangular element hydraulic gradients. Finally, we use DLEARN with this spatial distribution of body forces to compute the elastic effective stress field. This procedure is similar to that described by *Louis et al.* [1977].

Figure 2 illustrates the solution domain and boundary conditions used in each computation. The location of the bottom boundary deserves special attention because it can greatly influence the near-surface stress state predicted by elastic models. With a shallow bottom boundary having zero vertical displacement, numerical computations may yield a zone of near-surface tension near the apex of the slope [e.g., *Hoyaux and Landanyi*, 1972]. With a deeper bottom boundary, numerical computations may yield a zone of near-surface tension near the toe of the slope [e.g., *Zienkiewicz*, 1968]. Near-surface tension near the toe also occurs in some analytical solutions for bottom boundaries at an infinite depth [e.g., *Savage et al.*, 1985]. Our bottom boundary is located at a large depth (10 times the slope height), so that near-surface stress effects are similar to those obtained analytically for an infinitely deep elastic body.

TABLE 1. Nondimensionalization of Variables in Effective Stress Calculations

Quantity	Dimensions	Nondimensional Quantity
x, y (length)	L	x/H, y/H
ρ_t (total bulk density)	M/L^3	ρ_t/ρ_w
F (total body force)	M/L^2T^2	$F/\rho_w g$
σ'_{ij} (effective stress)	M/LT^2	$\sigma'_{ij}/\rho_w g H$

We investigated the accuracy of our numerical solutions in two ways: by comparing them with existing analytical solutions for topographically induced stress and by examining the effects of grid element size. Analytical solutions presented by *Savage et al.* [1985] determine the gravitational stress distribution under an isolated ridge or valley. Applying appropriate boundary conditions (i.e., boundaries far removed from the topographic relief), we generated numerical solutions that were very similar to these analytical solutions. For the periodic topography shown in Figure 1 we solved a series of identical problems with differing grid element sizes. On the basis of these tests we selected a grid of 1240 elements for the elastic displacement model and 1210 elements for the groundwater flow model. Near-surface element dimensions were approximately 1/20 times the slope height, whereas larger elements were used in the deeper regions. Displacements computed using these grids were within 5 percent of those calculated using a grid of 2480 elements.

Numerical Results

Here we present numerical results for a straight hillslope composed of homogeneous material and inclined 26.6 deg (2:1 slope). Results for this simple example illustrate basic influences of groundwater flow on the effective stress field due to topography. Parameter values for the hillslope material are those typical of soil: $\nu = 0.333$, ρ_t(dry) = 1590 kg/m^3, ρ_t(saturated) = 1990 kg/m^3, and ρ_w = 1000 kg/m^3 [cf. *Dunn et al.*, 1980]. Note that because the material is homogeneous, the value of the hydraulic conductivity K is inconsequential.

We use three techniques to reduce and present our numerical results: (1) nondimensionalization of variables; (2) conversion of effective stresses to principal effective stresses; and (3) expression of Coulomb failure potential by the ratio of the maximum shear stress to mean effective normal stress. We nondimensionalize the variables as shown in Table 1. Note that length is scaled by H, the height of the hillslope (Figure 2), body forces are scaled by $\rho_w g$, and effective stresses are scaled by $\rho_w g H$. To simplify the succeeding discussion, the term "stress" will hereinafter refer to effec-

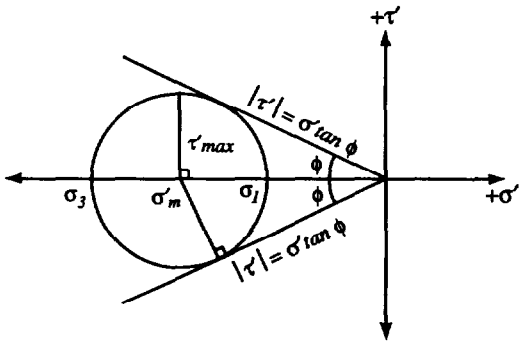

Fig. 3. Mohr stress diagram and Coulomb failure envelope for cases in which normal stresses are compressional but are defined as positive in tension.

tive stress, and nondimensionalization of this stress is implicit in all computational results.

We use standard relationships to obtain principal stresses from our computed stresses σ'_{xx}, σ'_{yy}, and σ'_{xy} [*Hughes*, 1987]:

$$\sigma_1 = \frac{\sigma'_{xx} + \sigma'_{yy}}{2} + \sqrt{\left(\frac{\sigma'_{xx} - \sigma'_{yy}}{2}\right)^2 + \sigma'^2_{yx}} \qquad (20a)$$

$$\sigma_3 = \frac{\sigma'_{xx} + \sigma'_{yy}}{2} - \sqrt{\left(\frac{\sigma'_{xx} - \sigma'_{yy}}{2}\right)^2 + \sigma'^2_{yx}} \qquad (20b)$$

The principal stresses σ_1 and σ_3 represent the maximum and minimum normal stresses, which act on planes where the shear stress is zero. The directions in which the principal stresses act are rotated from the x-y axes by an angle β:

$$\beta = \tfrac{1}{2} \arctan\left(\frac{2\sigma'_{yx}}{\sigma'_{xx} - \sigma'_{yy}}\right) \qquad (21)$$

Normal and shear stresses on any arbitrarily oriented plane can be found from the magnitude and orientation of the principal stresses. Thus the principal stresses provide a complete picture of the stress field.

Specifically, we are interested in the stresses that influence the potential for shear failure. Shear failure of cohesionless earth materials is described well by the Coulomb failure rule, which can be written in the form:

$$\frac{\sigma_1 - \sigma_3}{\sigma_1 + \sigma_3} = \frac{|\tau'_{\max}|}{-\sigma'_m} = \sin\phi \qquad (22)$$

where $\tau'_{\max}$ is the maximum shear stress, σ'_m is the mean normal stress (positive in tension), and ϕ is the angle of internal friction [*Lambe and Whitman*, 1979, p. 141]. The Coulomb rule assumes that the intermediate principal stress σ_2 does not influence failure. A graphical representation of (22) and its relationship to other forms of the Coulomb failure rule are shown by a Mohr diagram in Figure 3. We neglect the effects of cohesion because they would introduce scale dependence in our analysis. Moreover, the effects of cohesion are relatively unimportant for our purposes, because cohesion is not influenced by groundwater flow.

Determination of the orientation and magnitude of the stresses acting on a failure plane requires knowledge of the angle of internal friction. However, the stress ratio $|\tau'_{\max}|/(-\sigma'_m)$ that appears in the Coulomb failure rule (equation (22)) can be evaluated without this knowledge. We therefore define the Coulomb failure potential Φ as a dimensionless measure of shear failure potential:

$$\Phi = \frac{|\tau'_{\max}|}{-\sigma'_m} \qquad (23)$$

The value of Φ is independent of the material strength and has a theoretical minimum of zero and maximum of one.

An alternate mode of failure exists if either principal stress is tensile. Then, regardless of shear stress values, cohesionless Coulomb materials will fail. In this case the value of Φ is unimportant, and we simply identify the affected region as being tensional.

Stresses in a Dry Hillslope

Figure 4 depicts the principal stresses in a dry elastic hillslope with a uniform gravitational body force. All stresses are compressional. The complete solution domain, not all of which is shown in Figure 4, extends to a depth of 10 times the hillslope height. Near the surface, the orientation of the maximum compressive stress roughly parallels the ground surface. At depth, the direction of maximum compression becomes vertical, aligned with gravity.

The values of the failure potential Φ within the same dry hillslope are contoured in Figure 5. Regions of high Φ occur in a thin band subparallel and adjacent to the ground surface. Values of Φ within this band are approximately uniform, except at the lateral boundaries where Φ is smaller because of constraints on horizontal displacement.

Body Forces in a Saturated Hillslope

When the same hillslope is saturated, gravity-driven groundwater flow occurs. The resulting normalized seepage forces (specified mathematically by $-\nabla h$) are portrayed in Figure 6. These seepage-induced body forces are largest

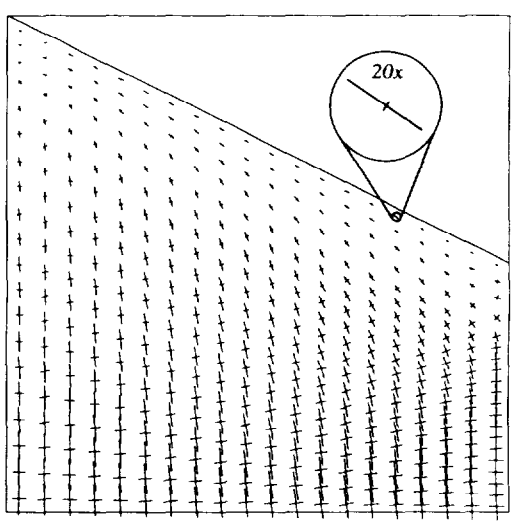

Fig. 4. Orientation and magnitude of principal stresses in a dry, homogeneous, elastic hillslope. All stresses are compressional. The length of each orthogonal line in the stress symbols equals the magnitude of the nondimensional stress in that direction multiplied by a plotting factor of 0.05.

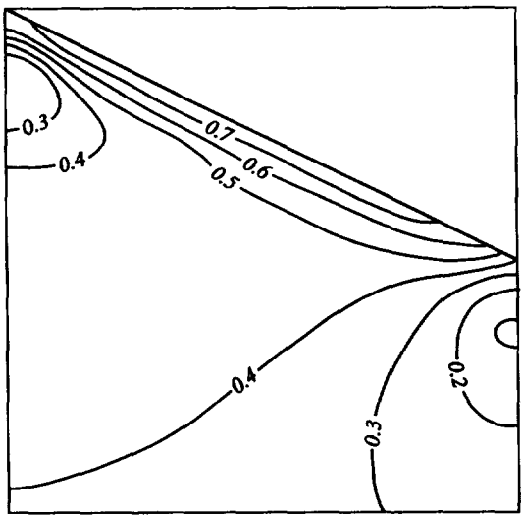

Fig. 5. Distribution of the Coulomb failure potential Φ determined from the dry hillslope stress field of Figure 4.

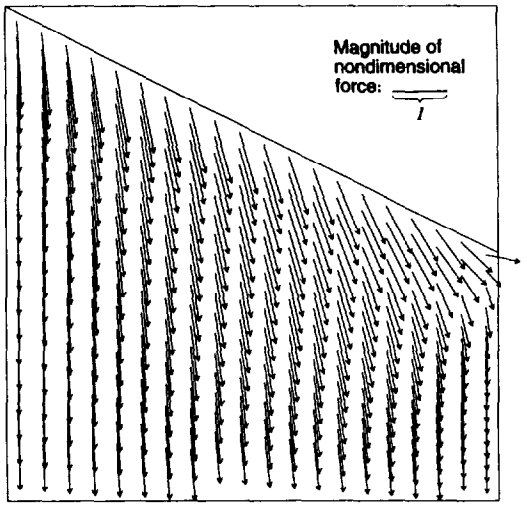

Fig. 7. Nondimensional total body force field in a saturated, homogeneous hillslope with gravity-driven groundwater flow.

near the surface and are negligible at depth. All have a horizontal component oriented downslope. Near the top of the slope, the seepage forces have a downward vertical component in the direction of gravitational attraction, whereas near the toe of the slope, they have an upward component that acts against gravity.

The combination of seepage body forces with gravitational and buoyancy body forces produces the net body force field shown in Figure 7. Although gravity and buoyancy act vertically downward and upward, respectively, seepage adds a horizontal component that is most significant near the ground surface (Figure 6). Seepage has the largest effect on body forces at the toe of the slope, where it has components that act both downslope and against gravity.

Stresses in a Saturated Hillslope

The principal stresses in a saturated elastic hillslope with the body force field of Figure 7 are shown in Figure 8.

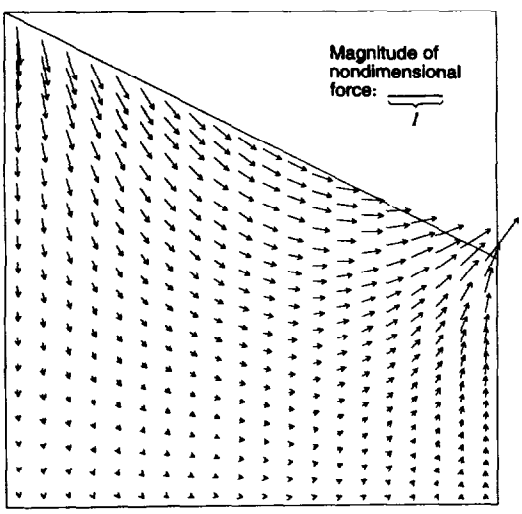

Fig. 6. Nondimensional seepage force field in a saturated, homogeneous hillslope with gravity-driven groundwater flow.

Although these stresses are broadly similar to those in the dry hillslope (Figure 4), important differences exist. Buoyancy effects reduce the vertical compression throughout the domain. Because the near-surface seepage forces have a downslope component, near-surface lateral compression is larger. In addition, seepage forces rotate the orientation of the principal stresses, most notably near the toe of the slope.

In the saturated hillslope the failure potential Φ generally exceeds that in the dry slope (Figure 9). Near the slope toe, where seepage is directed outward, Φ is particularly large and approaches its theoretical maximum of 1. The region with a high Φ value also extends deeper than in the dry hillslope, and it is shifted in the downslope direction. This deepening and downslope shifting can be clearly seen by comparing the 0.7 contours in Figures 5 and 9. All of the changes in Φ are caused by seepage effects, because buoy-

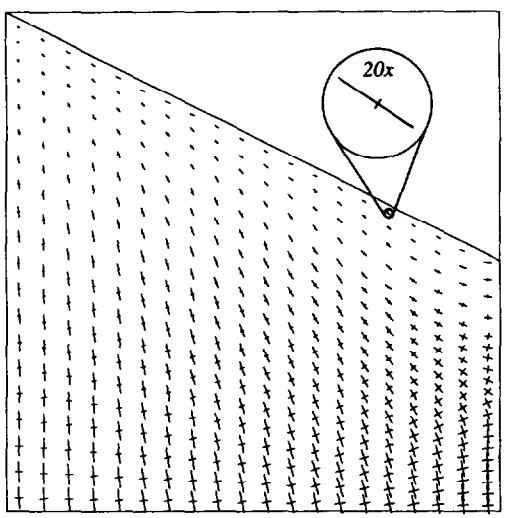

Fig. 8. Principal effective stresses in a saturated, homogeneous, elastic hillslope with gravity-driven groundwater flow. All stresses are compressional. The length of each line in the stress symbols represents the magnitude of the nondimensional stress in that direction multiplied by a plotting factor of 0.05.

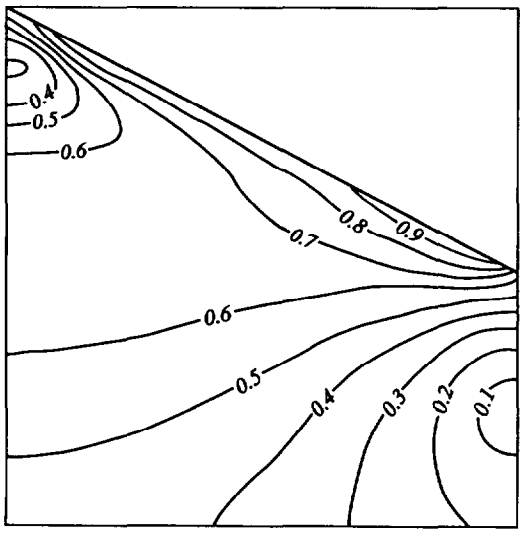

Fig. 9. Distribution of the Coulomb failure potential Φ determined from the saturated hillslope effective stress field of Figure 8.

ancy forces alone merely reduce the apparent weight of the solids and do not change the magnitude of Φ.

The percent increase in Φ between the dry and saturated hillslopes is shown in Figure 10. Because there is a horizontal body force component in the saturated case (Figure 7), values of Φ change greatly near the lateral boundaries, where displacement of adjacent material cannot help distribute the stress caused by groundwater flow. However, in the region of interest near the surface of the slope the percent increase in Φ is greatest near the slope toe.

Contrast With One-Dimensional Analysis

Some key features of the foregoing results are revealed by contrasting them with results for an analogous one-dimensional problem. Such one-dimensional, "infinite slope" problems assume that the slope is a free body unaffected by lateral boundaries and that body forces and

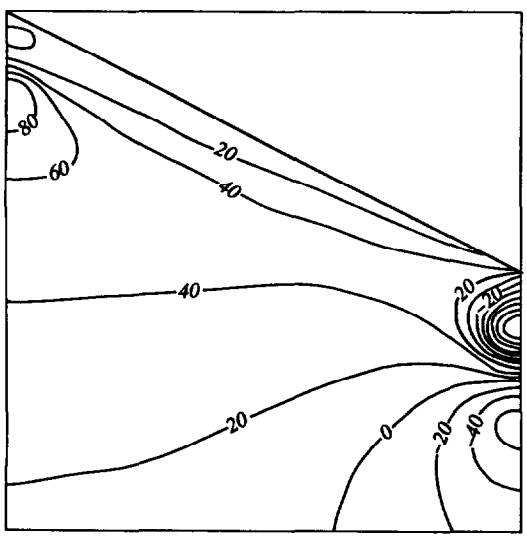

Fig. 10. Percent increase in the failure potential Φ between dry and saturated cases (Figures 5 and 9).

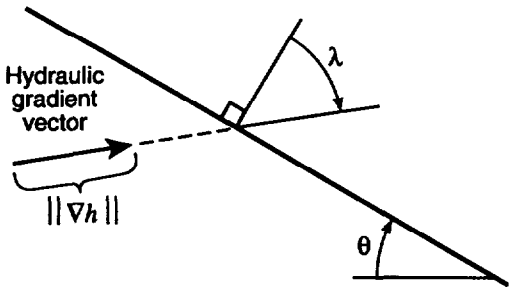

Fig. 11. Definition of the angular direction (λ) and scalar magnitude ($\|\nabla h\|$) of the hydraulic gradient vector (pointing in the direction of $-\nabla h$) in an infinite slope.

effective stresses vary only as functions of a coordinate oriented normal to the slope surface [*Iverson and Major*, 1986; *Iverson*, 1992]. This restricts the variety of groundwater flow fields that are compatible with an infinite slope analysis [*Iverson*, 1990].

Infinite slope analyses are instructive, however, because they are statically determinate and yield a one-dimensional Coulomb failure potential Φ_{1D} that is both uniform throughout the slope and closely related to a limit equilibrium factor of safety. In infinite slopes, potential failure planes must parallel the slope surface, and the Coulomb failure rule for cohesionless materials is expressed in terms of the effective normal and shear stresses on these planes, σ' and τ' [*Lambe and Whitman*, 1979, p. 141]:

$$|\tau'| = \sigma' \tan \phi \tag{24}$$

We thus define the one-dimensional failure potential Φ_{1D} as

$$\Phi_{1D} = \frac{|\tau'|}{\sigma'} \tag{25}$$

and the factor of safety FS as

$$FS = \frac{\sigma' \tan \phi}{|\tau'|} = \frac{\tan \phi}{\Phi_{1D}} \tag{26}$$

The one-dimensional failure potential is analogous, but not identical, to the two-dimensional failure potential Φ.

To obtain a more useful expression for Φ_{1D}, we use the results of *Iverson and Major* [1986] and substitute explicit expressions for τ' and σ' into (25). The resulting equation applies to saturated infinite slopes with seepage forces of any magnitude and direction:

$$\Phi_{1D} = \frac{[(\rho_t/\rho_w) - 1] \sin \theta + \|\nabla h\| \sin \lambda}{[(\rho_t/\rho_w) - 1] \cos \theta - \|\nabla h\| \cos \lambda} \tag{27}$$

Here $\|\nabla h\|$ is the magnitude and λ the angular direction of the hydraulic gradient vector, and θ is the slope angle (Figure 11). For infinite slopes with a water table at the ground surface it is necessary that $\|\nabla h\| = |\sin \theta / \sin \lambda|$; and for saturated flow it is necessary that $0 \leq \lambda \leq 180° - \theta$ [*Iverson*, 1992]. Under these constraints, (27) simplifies to

$$\Phi_{1D} = [\cot \theta - (\rho_w/\rho_t)(\cot \theta + \cot \lambda)]^{-1} \tag{28}$$

Figure 12 depicts solutions of (27), as well as the solution of (28), for an infinite slope with the same inclination (θ = 26.6°) and mass-density ratio (ρ_t/ρ_w = 1.99) used in our

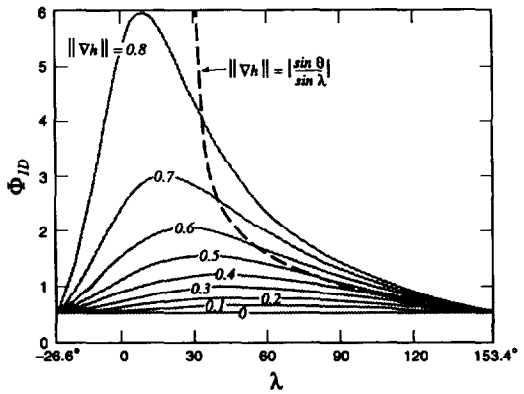

Fig. 12. One-dimensional Coulomb failure potential Φ_{1D} as a function of the direction and magnitude of the hydraulic gradient vector in an infinite slope with $\rho_t/\rho_w = 1.99$, slope angle $\theta = 26.6°$, and uniform groundwater flow. Solid lines represent solutions of (27) for all possible values of λ, with $\|\nabla h\| \leq 0.8$. Heavy dashed line represents solution of equation (28), which incorporates the restriction that a water table boundary exists at the ground surface. Solutions of (28) indicate that Φ_{1D} grows without bound as λ diminishes toward 26.9°.

two-dimensional example (Figures 6–10). These solutions show how the Coulomb failure potential Φ_{1D} varies as a function of the magnitude and direction of the hydraulic gradient. If groundwater flow is vertically upward ($\lambda = -26.6°$) or downward ($\lambda = 153.4°$) Figure 12 shows that the seepage force merely changes the apparent weight of the solids and does not influence the Coulomb failure potential. However, if groundwater flow has a downslope component, as it does throughout the domain in our two-dimensional example (Figure 6), Figure 12 shows that the failure potential is increased. Moreover, the influence of seepage on the one-dimensional failure potential is far greater than in the two-dimensional case. Seepage forces similar to those near the toe of the slope in Figure 6 (for example, $\lambda = 35°$, $\|\nabla h\| = 0.8$), would produce a one-dimensional failure potential that exceeded the dry-slope potential by more than 600%. Instead, such seepage forces increase the failure potential by only about 40% in the two-dimensional case (Figure 10). This smaller effect on failure potential results from the spatial variability of the two-dimensional groundwater flow and stress fields; continuity of these fields helps restrain the material in zones where the failure potential would otherwise be extremely high.

Discussion

This discussion focuses first on some general inferences about groundwater effects on stress distributions and failure potentials in hillslopes. Then, we discuss our use of linear elasticity for modeling stresses and our use of Φ for evaluating failure potential, and we contrast this approach with some alternative approaches. We explain why caution should be used in drawing unequivocal conclusions on the basis of our model results.

The principal result of our numerical computations is a conceptual picture of how groundwater flow modifies static effective stresses in hillslopes. As a backdrop for this picture, the body force terms in the governing equations show that spatially uniform changes in pore pressure do not influence the effective stress state or failure potential. Consequently, the idea that high pore pressures cause slope failure can be very misleading. Instead, it is the distribution of pore pressures that deviate from hydrostatic that influences failure potential. The effects of this distribution are represented by the direction and magnitude of seepage forces.

Our results also show that groundwater flow fields influence both shear stresses and effective normal stresses. This contradicts the view, apparently derived from effective stress definitions such as (8) or (11), that pore fluid pressures affect only normal stresses [e.g., *Hubbert and Rubey*, 1959]. Although pore fluid can support no static shear stress itself, flowing pore fluid can impart static shear stress to the solids. This effect can be appreciated on an intuitive level by considering the net body force field that exists when gravity-driven groundwater flow occurs (Figure 7). Because the groundwater flow field produces curvature of the net body force field, the porous medium sustains stresses that include shear as well as normal components. Definitions of effective stress do not reveal this effect. Solutions to boundary value problems, either in terms of seepage forces, as we have presented here, or in terms of pore pressure distributions, must be examined to evaluate groundwater effects on effective stress fields.

For straight hillslopes composed of homogeneous material our effective stress and failure potential calculations show that a rational expectation is for failures to be shallow, involving only material near the slope surface. In this near-surface region, both shear and normal stresses are strongly influenced by the traction-free boundary condition at the ground surface. In addition, gravity-driven groundwater flow increases the failure potential in the near-surface region, and the increases are largest near the toe of the slope. This is a consequence of seepage forces directed outward from the slope near the toe; it suggests that slope failure might be expected to nucleate in this region.

Localized effects of groundwater flow on failure potential are less pronounced, however, than might be expected on the basis of solutions to analogous one-dimensional problems [e.g., *Iverson and Major*, 1986; *Iverson*, 1992]. In one-dimensional problems, seepage and attendant stress field modification uniformly affect a mechanically isolated domain. In contrast, our two-dimensional solutions must satisfy compatibility conditions and boundary constraints on displacements and groundwater flow. No part of the solution domain is isolated from any other part, and the contiguity of all parts mediates the localized influences of groundwater flow.

The role of domain contiguity points to contrasts between our approach and the commonly used limit equilibrium method of slope stability analysis. Our approach uses the distribution of elastic stresses to evaluate the effect of groundwater flow on the distribution of Coulomb failure potential Φ in a continuous domain. Inferences about groundwater effects on the failure potential are broadly applicable because there are no assumptions about failure plane locations or material frictional strength. However, the failure potential Φ cannot be translated directly into factor-of-safety and failure surface predictions.

If factors of safety for potential failure surfaces are desired, the customary approach is limit equilibrium analysis. Such analyses have great engineering utility, but they yield a

limited view of groundwater influences on effective stress states because they assess only the net force balance on an isolated piece of a slope. This isolated free body is separated from the rest of the slope by an assumed failure surface, and the state of stress and pore water pressures at locations not on the failure surface are inconsequential. Zones inside or outside the failure surface that may be weakened by the effects of groundwater flow are irrelevant. Thus despite its advantages for practical assessments of slope stability, limit equilibrium analysis yields no coherent picture of groundwater effects that is comparable to our Figure 10.

Our stress field calculation method requires that rock or soil deformation is linearly elastic prior to failure. Responses of soil and rock to short-term stresses are typically both linear and elastic [*Jaeger and Cook*, 1979], but responses to long-term loads may include creep deformation and concomitant stress relaxation. Our model does not include such time-dependent effects; it assumes that a landscape exists independent of its constructional or erosional history, that the only force affecting the landscape is the time-independent action of gravity, and that stresses and groundwater flow equilibrate to this gravitational force instantaneously and permanently.

The validity of such time-independent elastostatic stress calculations has been questioned by *McGarr* [1987, 1988], who argued that basic modeling assumptions, particularly "switching on" gravity after lithification and imposing lateral constraints on displacement, do not mimic the evolution of earth materials. He suggested that a lithostatic stress state might be more appropriate. However, stress measurements near the Earth's surface are equivocal; horizontal stresses may be lower, equal to, or higher than vertical stresses [e.g., *Hooker et al.*, 1972; *McGarr and Gay*, 1978; *Jaeger and Cook*, 1979; *Swolfs and Savage*, 1985]. In light of this evidence, care should be taken in interpreting any stress field calculations, including our own. Nonetheless, our assumption of stresses governed by linear elasticity combines the advantages of being explicit, simple, and mechanically rational. Moreover, our focus is on modification of stress fields by groundwater flow and not on precise determination of the stress state. It is in this context that we believe our results have their greatest value.

Conclusions

The results of this study support the following conclusions. The first three conclusions are general; their applicability is demonstrated by equations that do not depend on any of our assumptions about elastic material behavior or our definition of failure potential. The last four conclusions are more specific and depend on our modeling assumptions.

1. Spatially uniform pore pressure changes, which have no influence on groundwater flow, also have no influence on effective stress distributions and failure potential in hillslopes. This is true regardless of pore pressure magnitudes.
2. Gravity-driven groundwater flow produces a spatially variable body force field that influences the effective stress distribution in hillslopes.
3. Shear stresses, as well as effective normal stresses, in a porous medium can be influenced by groundwater flow.
4. A general picture of groundwater effects on slope failure potential, which avoids the assumptions of limit equilibrium analysis, can be obtained by evaluating elastic effective stresses and calculating the distribution of the failure potential Φ throughout the slope.
5. Gravitational effects, by themselves, produce elastic stresses with magnitudes and orientations that are influenced by topography. Failure potentials due to these gravitational stresses show that near-surface failures are a rational expectation for straight, homogeneous slopes with no groundwater flow.
6. In straight, homogeneous slopes the failure potential is increased in near-surface parts of the slope as a result of gravity-driven groundwater flow. The increases are particularly significant near the slope toe, where seepage forces are strong and directed outward.
7. Increases in failure potential caused by gravity-driven groundwater flow in a two-dimensional slope are less pronounced than might be anticipated on the basis of infinite slope limit equilibrium calculations. This reflects the influence of compatibility, continuity, and boundary constraints on the two-dimensional groundwater flow and stress fields.

Appendix A: Steady State Decoupling

This appendix shows that under steady state conditions the equations that govern flow of a homogenous, incompressible fluid in a heterogeneous, poroelastic medium decouple from the equations that govern the solid-state stress field. The derivation focuses on the case of two-dimensional flow and plane strain considered in this paper, but it can easily be generalized to three dimensions.

As a starting point, we consider the poroelastic constitutive equations for plane strain derived by *Rice and Cleary* [1976, equation (20)), which are valid for fully coupled solid and fluid deformation. The first of their equations is a slightly different form of (B5) presented in this paper; it differs in that it does not require the assumption of incompressible pore fluid. The second of their equations relates the mass of pore fluid contained in a representative volume of the porous medium to the state of stress:

$$m - m_0 = \frac{3\rho_0(\nu_u - \nu)}{2GB(1 + \nu_u)}\left[(\sigma_{xx} + \sigma_{yy}) + \frac{3p^*}{B(1 + \nu_u)}\right] \quad \text{(A1)}$$

Here ν_u is the undrained Poisson's ratio of the porous medium, B is Skempton's pore-pressure coefficient for the medium, m is the mass of pore fluid per unit volume of the medium, m_0 is a constant value of m measured at some reference state, and ρ_0 is a constant value of ρ_w measured at the same reference state. We assume that the pore fluid is incompressible so that $\rho_0 = \rho_w$ everywhere. The symbol p^* denotes the nonequilibrium pore fluid pressure, which is related to the hydraulic head h and total pore pressure p by

$$p^* = \rho_w g h = p + \rho_w g y \quad \text{(A2)}$$

Thus p^* reflects the total mechanical potential of the pore fluid. Note that body forces are omitted by *Rice and Cleary*'s [1976] derivation, so that they use $p^* = p$.

Using p^* as given by (A2) as the dependent variable, Darcy's law can be employed in the form

$$q_i = -(K/a)\frac{\partial p^*}{\partial x_i} \quad \text{(A3)}$$

in which q_i is the fluid mass flux per unit area of porous medium. Conservation of pore fluid mass during transient flow is then expressed by

$$\frac{\partial q_i}{\partial x_i} + \frac{\partial m}{\partial t} = 0 \tag{A4}$$

in which t represents time. Substitution of (A1) and (A3) into (A4) then yields a diffusion equation for transient flow of homogeneous fluid in a heterogeneous poroelastic medium

$$\frac{1}{\rho_0 g}\frac{\partial}{\partial x_i}\left(K\frac{\partial p^*}{\partial x_i}\right) = \frac{3(\nu_u - \nu)}{2GB(1+\nu_u)} \cdot \frac{\partial}{\partial t}\left[(\sigma_{xx}+\sigma_{yy}) + \frac{3p^*}{B(1+\nu_u)}\right] \tag{A5}$$

In (A5) the time derivative, which operates on both the stress field and the pore pressure field, vanishes under steady state conditions. Thus for steady state we have

$$\frac{1}{\rho_0 g}\frac{\partial}{\partial x_i}\left(K\frac{\partial p^*}{\partial x_i}\right) = 0 \tag{A6}$$

Employing (A2) and the relation $\rho_0 = \rho_w$, and writing the x and y direction derivatives explicitly, (A6) reduces to

$$\frac{\partial}{\partial x}\left(K\frac{\partial h}{\partial x}\right) + \frac{\partial}{\partial y}\left(K\frac{\partial h}{\partial y}\right) = 0 \tag{A7}$$

This equation is the same as (15) for steady groundwater flow given in the main text. Effects of poroelastic coupling on fluid flow, which are commonly important in transient problems [*Roeloffs*, 1988], consequently are irrelevant in the steady state problems we consider here. Numerical analysis can therefore proceed by first determining the groundwater flow field, which subsequently serves as input for determining the elastic stress field.

Appendix B: Constitutive Equations

This appendix shows how constitutive equations similar to (9*a*)–(9*c*) are obtained from the poroelastic constitutive equations of *Biot* [1941], as recast by *Rice and Cleary* [1976]. The three-dimensional constitutive equation (equation (1)) of *Rice and Cleary* [1976] is

$$\varepsilon_{ij} = \frac{1}{2G}\left[\sigma_{ij} + p\delta_{ij} - \frac{\nu}{1+\nu}(\sigma_{kk}+3p)\delta_{ij} - \frac{2G}{3K_s'}p\delta_{ij}\right] \tag{B1}$$

in which G is the shear modulus of the solid porous medium and the other variables and moduli are defined as in the main text. The indices i, j, and k represent the coordinates x, y, and z, and the summation convention applies to repeated i, j, k indices. The modulus K_s' defined by Rice and Cleary differs somewhat from K_s, the bulk modulus of the solid constituents defined in the main text. However, we assume here that all pore spaces in the solid are interconnected and permit fluid flow, which implies that $K_s' = K_s$ [*Rice and Cleary*, 1976].

A well-known identity relates the shear modulus to the bulk modulus and Poisson's ratio of the solid skeleton [cf. *Fung*, 1965, p. 129]:

$$\frac{2G}{3} = K_b\left(\frac{1-2\nu}{1+\nu}\right) \tag{B2}$$

Substituting (B2) into (B1) and manipulating the resulting terms produces

$$\varepsilon_{ij} = \frac{1}{2G}\left\{\sigma_{ij} + \left(1-\frac{K_b}{K_s}\right)p\delta_{ij} - \frac{\nu}{1+\nu}\left[\sigma_{kk} + 3\left(1-\frac{K_b}{K_s}\right)p\right]\delta_{ij}\right\} \tag{B3}$$

Applying the plane strain definition, $\varepsilon_{zi} = 0$, reduces (B3) to the following expression for the out-of-plane stress σ_{zz}:

$$\sigma_{zz} = -\left(1-\frac{K_b}{K_s}\right)p + \frac{\nu}{1+\nu}\left[\sigma_{xx}+\sigma_{yy}+\sigma_{zz}+3\left(1-\frac{K_b}{K_s}\right)p\right]$$

$$= \nu(\sigma_{xx}+\sigma_{yy}) - (1-2\nu)\left(1-\frac{K_b}{K_s}\right)p \tag{B4}$$

This equation is the total stress equivalent of the effective stress equation for plane strain (10) used in the main text. Substituting (B4) into (B3) yields, after some algebraic manipulation,

$$\varepsilon_{ij} = \frac{1}{2G}\left[\sigma_{ij} - \nu(\sigma_{xx}+\sigma_{yy})\delta_{ij} + (1-2\nu)\left(1-\frac{K_b}{K_s}\right)p\delta_{ij}\right] \tag{B5}$$

This is the general constitutive equation for plane strain.

Conversion of (B5) into a form very similar to that of (9*a*)–(9*c*) is then accomplished by using the definition [*Fung*, 1965, p. 129]:

$$G = \frac{E}{2(1+\nu)} \tag{B6}$$

Note that this definition of the shear modulus identifies it as one of the Lame parameters that appear in the equations governing solid displacements (17*a*) and (17*b*). Substituting (B6) into (B5), and writing the x and y component equations explicitly then gives, for the normal and shear strains,

$$\varepsilon_{xx} = \frac{1}{E}\left[(1-\nu^2)\sigma_{xx} - \nu(1+\nu)\sigma_{yy} + (1+\nu)(1-2\nu)\left(1-\frac{K_b}{K_s}\right)p\right] \tag{B7a}$$

$$\varepsilon_{yy} = \frac{1}{E}\left[(1-\nu^2)\sigma_{yy} - \nu(1+\nu)\sigma_{xx} + (1+\nu)(1-2\nu)\left(1-\frac{K_b}{K_s}\right)p\right] \tag{B7b}$$

$$\varepsilon_{yx} = \frac{1+\nu}{E}\sigma_{yx} \tag{B7c}$$

The close analogy between these equations, which govern total stresses, and (9*a*)–(9*c*), which govern effective stresses, is apparent. It is easy to show that substitution of the *Nur and Byerlee* [1971] effective stress definition (8) into (9*a*)–(9*c*) yields (B7*a*)–(B7*c*) as equivalent expressions.

NOTATION

B Skempton's pore pressure coefficient for the solid porous medium, dimensionless;
E Young's modulus of the solid porous medium, M/LT^2;
F total body force, M/L^2T^2;
g magnitude of the gravitational acceleration vector, L/T^2;
g_i i component of the gravitational acceleration vector, L/T^2;
G shear modulus of the solid porous medium, M/LT^2;
h total groundwater head, L;
H hillslope height, L;
i, j, k dummy indices that represent the coordinates x, y and z;
K hydraulic conductivity, L/T;
K_b bulk modulus of the solid porous medium, M/LT^2;
K_s bulk modulus of the individual solid constituents, M/LT^2;
K'_s bulk modulus defined by *Rice and Cleary* [1976], M/LT^2;
m mass of pore water per unit volume of porous medium, M/L^3;
m_0 value of m at reference state, M/L^3;
n_i i component of the unit normal vector directed outward from the slope surface, L;
p pore water pressure, M/LT^2;
p^* nonequilibrium pore water pressure, M/LT^2;
q_i i component of the fluid mass flow rate per unit area of porous medium, M/L^2T;
t time, T;
u_i i component of the solid porous medium displacement vector, L;
x, y, z Cartesian coordinates, L;
x_A value of x along right boundary of solution domain, L;
Y value of y along topographic surface, L;
α coefficient in effective stress definition, dimensionless;
β angle between directions of principal stress action and the x-y axes, dimensionless;
δ_{ij} Kronecker delta (= 1 when $i = j$ and = 0 otherwise), dimensionless;
ε_{ij} component of the infinitesimal solid strain tensor, dimensionless;
ϕ angle of internal friction, dimensionless;
Φ Coulomb failure potential, dimensionless;
Φ_{1D} one-dimensional Coulomb failure potential, dimensionless;
λ angular direction of hydraulic gradient vector, dimensionless;
ν drained Poisson's ratio of the porous medium, dimensionless;
ν_u undrained Poisson's ratio of the porous medium, dimensionless;
θ slope angle, dimensionless;
ρ_t total mass density of the solid-fluid mixture, M/L^3;
ρ_w mass density of pore water, M/L^3;
ρ_0 mass density of pore water at reference state, M/L^3;
σ_{ij} component of the total stress tensor, M/LT^2;
σ'_{ij} component of the effective stress tensor, M/LT^2;
σ' effective normal stress in infinite slope, M/LT^2;
σ_1, σ_3 major and minor principal effective stresses, M/LT^2;
σ'_m mean effective normal stress, M/LT^2;
τ' shear stress in infinite slope, M/LT^2;
τ'_{max} maximum shear stress, M/LT^2;
∇ gradient operator, $1/L$;
∇^2 Laplacian operator, $1/L^2$.

Acknowledgments. We thank Rex Baum, John Bredehoeft, Bill Haneberg, Bill Savage, and anonymous reviewers for comments that helped improve the manuscript. We thank Tom Hughes and Lynn Torak for introducing us to their respective finite element codes.

REFERENCES

Biot, M. A., General theory of three-dimensional consolidation, *J. Appl. Phys.*, *12*, 155–164, 1941.

Cooley, R. L., A review and synthesis of the Biot and Jacob-Cooper theories of ground-water motion, *Publ. 25*, Hydrol. and Water Resour., Desert Res. Inst., Reno, Nev., 1975.

Duncan, J. M., and P. Dunlop, Slopes in stiff-fissured clays and shales, *J. Soil Mech. Found. Div. Am. Soc. Civ. Eng.*, *95*(SM2), 467–492, 1969.

Dunn, I. S., L. R. Anderson, and F. W. Kiefer, *Fundamentals of Geotechnical Analysis*, John Wiley, New York, 1980.

Forster, C., and L. Smith, Groundwater flow systems in mountainous terrain, 1, Numerical modeling technique, *Water Resour. Res.*, *24*(7), 999–1010, 1988*a*.

Forster, C., and L. Smith, Groundwater flow systems in mountainous terrain, 2, Controlling factors, *Water Resour. Res.*, *24*(7), 1011–1023, 1988*b*.

Freeze, R. A., and J. A. Cherry, *Groundwater*, Prentice-Hall, Englewood Cliffs, N. J., 1979.

Freeze, R. A., and P. A. Witherspoon, Theoretical analysis of regional groundwater flow, 1, Analytical and numerical solutions to the mathematical model, *Water Resour. Res.*, *2*(4), 641–656, 1966.

Freeze, R. A., and P. A. Witherspoon, Theoretical analysis of regional groundwater flow, 2, Effect of water-table configuration and subsurface permeability variation, *Water Resour. Res.*, *3*(2), 623–634, 1967.

Fung, Y. C., *Foundations of Solid Mechanics*, Prentice-Hall, Englewood Cliffs, N. J., 1965.

Hodge, R. A., and R. A. Freeze, Groundwater flow systems and slope stability, *Can. Geotech. J.*, *14*, 466–476, 1977.

Hooker, V. E., D. L. Bickel, and J. R. Aggson, In situ determination of stresses in mountainous topography, *Rep. USBM RI 7654*, 19 pp., U.S. Bur. of Mines, 1972.

Hoyaux, B., and B. Landanyi, Stress distribution due to gravity in a vertical rock bank, *Proc. Symp. Rock Mech.*, *10*, 621–631, 1972.

Hubbert, M. K., and W. W. Rubey, Role of fluid pressure in mechanics of overthrust faulting, I, *Geol. Soc. Am. Bull.*, *70*, 115–166, 1959.

Hughes, T. J. R., *The Finite Element Method*, 803 pp., Prentice-Hall, Englewood Cliffs, N. J., 1987.

Iverson, R. M., Groundwater flow fields in infinite slopes, *Geotechnique*, *40*(1), 139–143, 1990.

Iverson, R. M., Sensitivity of stability analyses to groundwater data, in *Proceedings of the Sixth International Symposium on Landslides*, A. A. Balkeema, Rotterdam, Netherlands, in press, 1992.

Iverson, R. M., and J. J. Major, Groundwater seepage vectors and the potential for hillslope failure and debris flow mobilization, *Water Resour. Res.*, *22*(11), 1543–1548, 1986.

Iverson, R. M., and J. J. Major, Rainfall, ground-water flow, and seasonal movement at Minor Creek landslide, northwestern California: Physical interpretation of empirical relations, *Geol. Soc. Am. Bull.*, *99*(4), 579–594, 1987.

Jaeger, J. C., and N. G. W. Cook, *Fundamentals of Rock Mechanics*, 3rd Ed., Chapman and Hall, London, 1979.

Lambe, T. W., and R. V. Whitman, *Soil Mechanics*, SI Version, John Wiley, New York, 1979.

Louis, C., J.-L. Dessenne, and B. Feuga, Interaction between water flow phenomena and the mechanical behavior of soil or rock masses, in *Finite Elements in Geomechanics*, edited by G. Gudehus, pp. 479–511, John Wiley, New York, 1977.

Malvern, L. E., *Introduction to the Mechanics of a Continuous Medium*, Prentice-Hall, Englewood Cliffs, N. J., 1969.

McGarr, A., Comments on "Near-surface stress and displacement in a layered elastic crust" and "Stress in a stratified crust overlying a buried screw dislocation" by P. C. Leary, *J. Geophys. Res.*, *92*(B6), 4959–4964, 1987.

McGarr, A., On the state of lithospheric stress in the absence of applied tectonic forces, *J. Geophys. Res.*, *93*(B11), 13,609–13,617, 1988.

McGarr, A., and N. C. Gay, State of stress in the Earth's crust, *Ann. Rev. Earth Planet. Sci.*, *6*, 405–436, 1978.

McTigue, D. F., and C. C. Mei, Gravity-induced stresses near topography of small slope, *J. Geophys. Res.*, *86*(B10), 9268–9278, 1981.

Nash, D. F. T., A comparative review of limit-equilibrium methods of stability analysis, in *Slope Stability, Geotechnical Engineering and Geomorphology*, edited by M. G. Anderson and K. S. Richards, pp. 11–75, John Wiley, New York, 1987.

Nur, A., and J. D. Byerlee, An exact effective stress law for elastic deformation of rock with fluids, *J. Geophys. Res.*, *76*(B6), 6414–6419, 1971.

Passman, S. L., and D. F. McTigue, A new approach to the effective stress principle, in *Compressibility Phenomena in Subsidence*, edited by S. K. Saxena, pp. 79–91, Engineering Foundation, New York, 1986.

Patton, F. D., and A. J. Hendron, General report on mass movements, *Proceedings of the 2nd International Congress of the International Association of Engineering Geologists, Sao Paulo, Brazil*, vol. 2, pp. V-GR-1–V-GR-57, 1974.

Perloff, W. H., G. Y. Baladi, and M. E. Harr, Stress distribution within and under long elastic embankments, *Highw. Res. Rec.*, *181*, 12–40, 1967.

Phukan, A. L. T., K. Y. Lo, and P. LaRochelle, Stresses and deformations of vertical slopes in elasto-plastic rocks, *Proc. Symp. Rock Mech.*, *11*, 193–212, 1970.

Pinder, G. F., M. Celia, and W. G. Gray, Velocity calculation from randomly located hydraulic heads, *Ground Water*, *19*(3), 262–264, 1981.

Reid, M. E., and R. M. Iverson, Gravity-driven groundwater flow and slope failure potential, 2, Effects of slope morphology, material properties, and hydraulic heterogeneity, *Water Res. Res.*, this issue.

Reid, M. E., H. P. Nielsen, and S. J. Dreiss, Hydrologic factors triggering a shallow hillslope failure, *Bull. Assoc. Eng. Geol.*, *25*(3), 349–361, 1988.

Rice, J. R., and M. P. Cleary, Some basic stress diffusion solutions for fluid-saturated elastic porous media with compressible constituents, *Rev. Geophys. Space Phys.*, *14*(2), 227–241, 1976.

Roeloffs, E. A., Fault stability changes induced beneath a reservoir with cyclic variations in water level, *J. Geophys. Res.*, *93*(B3), 2107–2124, 1988.

Rulon, J. J., and R. A. Freeze, Multiple seepage faces on layered slopes and their implications for slope-stability analysis, *Can. Geotech. J.*, *22*, 347–356, 1985.

Sandhu, R. S., and E. L. Wilson, Finite-element analysis of seepage in elastic media, *J. Eng. Mech. Div. Am. Soc. Civ. Eng.*, *95*(EM3), 641–652, 1969.

Savage, W. Z., H. S. Swolfs, and P. S. Powers, Gravitational stresses in long symmetric ridges and valleys, *Int. J. Rock Mech. Min. Sci. Geomech. Abstr.*, *22*(5), 291–302, 1985.

Serafim, J. L., Influence of interstitial water on the behaviour of rock masses, in *Rock Mechanics in Engineering Practice*, edited by K. G. Stagg and O. C. Zienkiewicz, pp. 55–97, John Wiley, New York, 1968.

Silvestri, V., and C. Tabib, Exact determination of gravity stresses in finite elastic slopes, Part I, Theoretical considerations, *Can. Geotech. J.*, *20*, 47–54, 1983*a*.

Silvestri, V., and C. Tabib, Exact determination of gravity stresses in finite elastic slopes, Part II, Applications, *Can. Geotech. J.*, *20*, 55–60, 1983*b*.

Stagg, K. G., and O. C. Zienkiewicz, Pore pressure and stress distribution in a porous material (Editor's note), in *Rock Mechanics in Engineering Practice*, edited by K. G. Stagg and O. C. Zienkiewicz, pp. 86–89, John Wiley, New York, 1968.

Sturgul, J. R., A. E. Scheidegger, and Z. Grinshpan, Finite-element model of a mountain massif, *Geology*, *4*, 439–442, 1976.

Swolfs, H. S., and W. Z. Savage, Topography, stresses, and stability at Yucca Mountain, Nevada, *Proc. Symp. Rock Mech.*, *26*, 1121–1129, 1985.

Ter-Martirosyan, Z., and D. Akhpatelov, The stress state of an infinite slope with curvilinear boundary in the field of gravity and seepage (in Russian with English abstract), *J. Probl. Geomech.*, *5*, 81–91, 1972.

Terzaghi, K., Die Berechnung der Durchassigkeitsziffer des Tones aus dem Verlauf der hydrodynamischen Spannungsercheinungen, *Sitzungsber. Akad. Wiss. Wien Math. Naturwiss. Kl.*, Abt. 2A, *132*, 105–124, 1923.

Terzaghi, K., The shearing resistance of saturated soils, *Proc. Int. Conf. Soil Mech. Found. Eng.*, *1*, 54–55, 1936.

Timoshenko, S. P., and J. N. Goodier, *Theory of Elasticity*, 3rd ed., 567 pp., McGraw-Hill, New York, 1970.

Torak, L. J., A MODular Finite-Element (MODFE) program for two-dimensional and axisymmetric ground-water flow problems, part 2, Model description and users' manual, *U.S. Geol. Surv. Open File Rep. 90-194*, in press, 1992.

Toth, J., A theoretical analysis of groundwater flow in small drainage basins, *J. Geophys. Res.*, *68*(B6), 4795–4812, 1963.

Wright, S. G., F. H. Kulhawy, and J. M. Duncan, Accuracy of equilibrium slope stability analysis, *J. Soil Mech. Found. Div. Am. Soc. Civ. Eng.*, *99*(SM10), 783–791, 1973.

Zienkiewicz, O. C., Continuum mechanics as an approach to rock mass problems, in *Rock Mechanics in Engineering Practice*, edited by K. G. Stagg and O. C. Zienkiewicz, pp. 237–273, John Wiley, New York, 1968.

Zienkiewicz, O. C., *The Finite Element Method*, 3rd ed., 787 pp., McGraw-Hill, New York, 1977.

Zienkiewicz, O. C., C. Humpheson, and R. W. Lewis, A unified approach to soil mechanics (including plasticity and viscoplasticity), in *Finite Elements in Geomechanics*, edited by G. Gudehus, pp. 151–177, John Wiley, New York, 1977.

R. M. Iverson, U.S. Geological Survey, Cascades Volcano Observatory, 5400 MacArthur Blvd., Vancouver, WA 98661.

M. E. Reid, U.S. Geological Survey, 677 Ala Moana Blvd., Suite 415, Honolulu, HI 96813.

(Received January 24, 1991;
revised October 16, 1991;
accepted October 25, 1991.)